Multilevel fast multipole method based on a potential formulation for 3D electromagnetic scattering problems

Mandiaye Fall[1, 2,*], Salim Boutami[1], Alain Glière[1], Jerome Hazart[1] and Brian Stout[2]

[1] CEA, LETI, MINATEC Campus, 17 av. des Martyrs, F-38054 Grenoble, France

[2] Institut Fresnel, CNRS, Aix-Marseille Université, Campus de Saint-Jérôme, F-13013 Marseille, France

[*]Corresponding authors: mandiaye.fall@cea.fr

A Combination of the Multilevel Fast Multipole Method (MLFMM) and Boundary Element Method (BEM) can solve large-scale photonics problems of arbitrary geometry. A new MLFMM, based on a scalar and vector potential formulation, instead of the more conventional electric and magnetic field formulations, is described. The method can deal with multiple lossy or lossless dielectric objects of arbitrary geometry, be they are nested, in contact, or disperse. Several examples are used to demonstrate that this method is able to efficiently handle 3D photonic scatterers involving large numbers of unknowns. Absorption, scattering and extinction efficiencies of gold nanoparticle spheres, calculated by the MLFMM, are compared with Mie's theory. MLFMM calculations of the bistatic Radar Cross Section (RCS) of a gold sphere near the plasmon resonance and of a silica coated gold sphere are also compared with Mie theory predictions. Finally, the bistatic RCS of a nanoparticle gold-silver heterodimer, calculated with MLFMM is compared with unmodified BEM calculations.

OCIS codes: 000.3860, 000.4430, 260.2110, 260.3910, 290.5890, 250.5403.

1. INTRODUCTION

Modeling in micro and nanophotonics, essential for designing and optimizing advanced optical devices, requires fast and accurate resolution of Maxwell's equations in three dimensions. A variety of numerically based approaches have been developed to solve electromagnetic scattering problems in three dimensions involving multiple objects and mixed materials. Among these various techniques, let us mention in particular the Finite Element Method (FEM) [1] and Finite-Difference Time-Domain (FDTD) [2], both of which use volume formulations, and the Boundary Element Method (BEM) relying on the surface integral equation [3–9]. Conventional BEM involves unknown electric and magnetic surface currents interrelated via the electric and magnetic fields continuity conditions. The applicability of the standard BEM to large-scale problems, even with parallel computing implementations, is limited by the large memory allocation and long computation times required to store and solve the algebraic system of equations. The Fast Multipole Method (FMM) can be coupled with the BEM in order to alleviate these demands.

The FMM, introduced by Rokhlin and Greengard [10,11], has been the subject of several works in 2D and 3D electromagnetic calculations [12–16]. In order to reduce the appetite of the FMM for both memory and calculation time, several studies have been devoted to extending it to a Multilevel Fast Multipole Method (MLFMM) [17–26]. The ability of MLFMM to solve large-scale electromagnetic problems involving over a million unknowns has been demonstrated [19–23]. Work has also been carried out on the application of the MLFMM to both 2D and 3D electromagnetic scattering problems involving electrical conductors and dielectric objects [27–29]. Different combinations of electric and magnetic field continuity equations, leading to formulation variations, have been compared in [30–35]. More recently, BEM and MLFMM have also been applied to plasmonic scatterers [34–39].

In this paper, we present a new MLFMM, based on the BEM formulation proposed by Garcia de Abajo and Howie [40,41]. This original BEM formulation is based on scalar and vector potentials, rather than electric and magnetic fields. The unknowns are equivalent charges and surface currents leading to the true electromagnetic field. This BEM formulation has already been applied to a variety of systems, including plasmonic scatterers [42–44]. In the present work, for the first time to our knowledge, a MLFMM is applied to this potential based BEM, in order to reduce the memory and computation times for systems with large numbers of unknowns. The general form of the method is given, which can deal with multiple objects of arbitrary materials, whether they be lossy or lossless materials. The geometries of the objects are also quite general as they can be nested, in contact or distinct. The BEM discretization of the boundary integral leads to a linear algebraic system. The resulting matrix is neither symmetric nor Hermitian. In order to iteratively solve this problem by the Generalized Minimal Residual (GMRES) method [45], one needs a good preconditioner. This is obtained by an incomplete LU (iLU) factorization of the sparse matrix of near interactions.

In the last part of the article, several examples are used to demonstrate that this method is able to efficiently handle 3D photonic scatterers involving large numbers of unknowns. First, absorption, scattering and extinction efficiencies of several gold nanoparticle spheres, calculated by the MLFMM, are compared with Mie's theory. Next, the bistatic Radar Cross Section (RCS) of a gold sphere near the plasmon resonance and of a silica coated gold sphere, obtained by the MLFMM, are compared with the predictions of Mie's theory. Finally, the bistatic RCS of a nanoparticle gold-silver heterodimer, calculated with MLFMM, is compared with usual BEM calculations.

2. FORMULATIONS

A. Single lossy dielectric formulation

In this section, we present a summary of the formulation for a single lossy dielectric body (Fig. 1). Further details can be found in the seminal work [40,41].

We begin with the time harmonic Maxwell's equations with $\exp(-i\omega t)$ time dependence

$$\nabla \times \mathbf{E} - ik\,\mathbf{B} = 0, \qquad \nabla.\mathbf{B} = 0$$

$$\nabla \times \mathbf{H} + ik\,\mathbf{D} = \frac{\mathbf{j}}{c}, \qquad \nabla.\mathbf{D} = \rho \tag{1}$$

where $k = \omega/c$, $\mathbf{D} = \varepsilon(\mathbf{r},\omega)\,\mathbf{E}$ is the electric displacement and $\mathbf{B} = \mu(\mathbf{r},\omega)\,\mathbf{H}$ the magnetic induction. In a lossy media, the dielectric permittivity ε has a positive imaginary component.

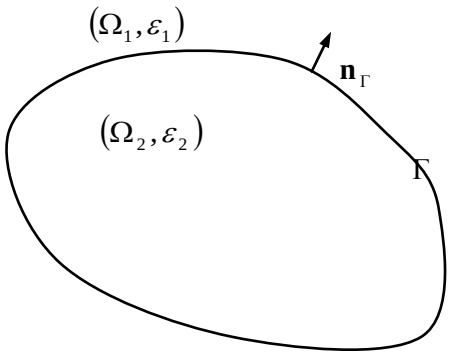

Fig. 1: The host medium is denoted Ω_1 and is characterized by a permittivity ε_1 (To remain consistent with Section B), while the volume inside the lossy dielectric body is denoted Ω_2 and characterized by ε_2. The interface between the two media is denoted Γ and the normal vector $\mathbf{n}_\Gamma$ is oriented towards Ω_1.

The first two equations in (1) are automatically satisfied by expressing $\mathbf{E}$ and $\mathbf{B}$ in terms of a scalar potential ϕ and vector potential $\mathbf{A}$:

$$\mathbf{E} = i\,k\,\mathbf{A} - \nabla\phi \tag{2}$$

$$\mu\,\mathbf{H} = \nabla \times \mathbf{A} \tag{3}$$

which are taken to also satisfy the Lorentz Gauge:

$$\nabla.\mathbf{A} = i\,k\varepsilon\mu\,\phi \tag{4}$$

Using these definitions, equations (1) take the form of two Helmholtz equations:

$$\left(\nabla + k^2\varepsilon\mu\right)\phi = -\left(\rho/\varepsilon - \sigma_\Gamma\right) \tag{5}$$

$$\left(\nabla + k^2\varepsilon\mu\right)\mathbf{A} = -\frac{1}{c}\left(\mu\,\mathbf{j} + \mathbf{h}_\Gamma\right) \tag{6}$$

The unknowns in equations (5) and (6) are $\mathbf{A}$, ϕ, σ_Γ and $\mathbf{h}_\Gamma$. The quantities σ_Γ and $\mathbf{h}_\Gamma$ are null inside the homogeneous regions (Ω_1 and Ω_2) and nonzero on the boundary surface (Γ). They can respectively be understood as additional charges and currents on the interface associated with the change in constitutive parameters. They are not the actual surface charges and currents, but produce the same scattered fields.

The general solutions of (5) and (6) are:

$$\phi(\mathbf{r}) = \phi_j^e(\mathbf{r}) + \int_\Gamma G_j\left(\left|\mathbf{r}-\mathbf{s}\right|\right)\sigma_j(\mathbf{s})d\mathbf{s}\,, \quad \forall\,\mathbf{r}\in\Omega_j,\ j=1,2 \tag{7}$$

$$\mathbf{A}(\mathbf{r}) = \mathbf{A}_j^e(\mathbf{r}) + \int_\Gamma G_j\left(\left|\mathbf{r}-\mathbf{s}\right|\right)\mathbf{h}_j(\mathbf{s})d\mathbf{s}\,, \quad \forall\,\mathbf{r}\in\Omega_j,\ j=1,2 \tag{8}$$

with

$$\phi_j^e(\mathbf{r}) = \frac{1}{\varepsilon_j(\omega)}\int_{\Omega_j} G_j\left(\left|\mathbf{r}-\mathbf{r}'\right|\right)\rho(\mathbf{r}')d\mathbf{r}' \tag{9}$$

$$\mathbf{A}_j^e(\mathbf{r}) = \frac{\mu_j(\omega)}{c}\int_{\Omega_j} G_j\left(\left|\mathbf{r}-\mathbf{r}'\right|\right)\mathbf{j}(\mathbf{r}')d\mathbf{r}' \tag{10}$$

where G_j is the scalar Green's function, given by

$$G_j\left(\left|\mathbf{r}\right|\right) = \frac{\exp\left(ik_j\left|\mathbf{r}\right|\right)}{4\pi\left|\mathbf{r}\right|} \quad , \quad \mathbf{r}\in\Omega_j \tag{11}$$

where $k_j = k\sqrt{\varepsilon_j(\omega)}$ is the wave number of the medium. The index *j* can take the values int(2) or out(1) respectively in the interior and exterior materials.

One remarks that the first terms on the right hand side of equations (7) and (8) are volume integrals, while the second terms are boundary integrals, since σ_Γ and $\mathbf{h}_\Gamma$ lie on the interface

between Ω_1 and Ω_2. The objective is to determine the equivalent surface charges and currents that produce electromagnetic fields satisfying appropriate boundary conditions.

The imposed boundary conditions at the interfaces are the continuity conditions on electric and magnetic fields, which are converted to continuity conditions on the scalar and vector potentials. After some algebraic manipulations [41], one finds the following matrix system:

$$\left[\mathbf{G}_{\text{int}}\right]\sigma_{\text{int}} - \left[\mathbf{G}_{out}\right]\sigma_{out} = \phi^{e}_{out} - \phi^{e}_{\text{int}} \tag{12}$$

$$\left[\mathbf{G}_{\text{int}}\right]\mathbf{h}_{\text{int}} - \left[\mathbf{G}_{out}\right]\mathbf{h}_{out} = \mathbf{A}^{e}_{out} - \mathbf{A}^{e}_{\text{int}} \tag{13}$$

$$[\mathbf{H}_{\text{int}}]\mathbf{h}_{\text{int}} - [\mathbf{H}_{out}]\mathbf{h}_{out} - ik\,\mathbf{n}_T\left(\left[\mathbf{G}_{\text{int}}\right]\varepsilon_{\text{int}}\sigma_{\text{int}} - \left[\mathbf{G}_{out}\right]\varepsilon_{out}\sigma_{out}\right) = \boldsymbol{\alpha} \tag{14}$$

$$[\mathbf{H}_{\text{int}}]\varepsilon_{\text{int}}\sigma_{\text{int}} - [\mathbf{H}_{out}]\varepsilon_{out}\sigma_{out} - ik\,\mathbf{n}_T.\left(\left[\mathbf{G}_{\text{int}}\right]\varepsilon_{\text{int}}\,\mathbf{h}_{\text{int}} - \left[\mathbf{G}_{out}\right]\varepsilon_{out}\mathbf{h}_{out}\right) = D^{e} \tag{15}$$

where the terms $\boldsymbol{\alpha}$ and D^{e} on the right hand side of these equations have explicit expressions in terms of the vector and scalar potentials at the interface [41]:

$$\boldsymbol{\alpha} = \left(\mathbf{n}_{\Gamma}.\nabla_{\Gamma}\right)\left(\mathbf{A}^{e}_{out} - \mathbf{A}^{e}_{\text{int}}\right) + ik\,\mathbf{n}_{\Gamma}\left(\varepsilon_{\text{int}}\mu_{\text{int}}\,\phi^{e}_{\text{int}} - \varepsilon_{out}\mu_{out}\,\phi^{e}_{out}\right)$$

$$D^{e} = \mathbf{n}_{\Gamma}.\left[\varepsilon_{\text{int}}\left(ik\,\mathbf{A}^{e}_{\text{int}} - \nabla_{\Gamma}\phi^{e}_{\text{int}}\right) - \varepsilon_{out}\left(ik\,\mathbf{A}^{e}_{out} - \nabla_{\Gamma}\phi^{e}_{out}\right)\right]$$

The $\left[\mathbf{G}_{\text{int}}\right]$ and $\left[\mathbf{H}_{\text{int}}\right]$ are the internal interactions matrices while $\left[\mathbf{G}_{out}\right]$ and $\left[\mathbf{H}_{out}\right]$ are the external interactions matrices. $\left[\mathbf{G}_{j}\right]$ and $\left[\mathbf{H}_{j}\right]$ are respectively related to Green's function G_j and its normal derivative. Their components are given by

$$\left[\mathbf{G}_{j}\right]_{a,b} = \int_{T_b} G_j\left(\left|\mathbf{s}_a - \mathbf{s}\right|\right)d\mathbf{s} \quad ,\mathbf{s}_a \in T_a \tag{16}$$

$$\left[\mathbf{H}_{j}\right]_{a,b} = \int_{T_b} \mathbf{n}_{T_a}.\nabla_{T_a} G_j\left(\left|\mathbf{s}_a - \mathbf{s}\right|\right)d\mathbf{s} \quad ,\mathbf{s}_a \in T_a \tag{17}$$

where $j = \text{int}, out$. The surface of the lossy dielectric body is discretized in triangles T and the unknown equivalent surface currents and charges are located at the center of mass [41]. The indices a and b respectively stand for the observation and source triangles.

B. Multiple lossy dielectric formulation

This section presents the extension of the previous formulation to multiple lossy dielectric objects (Fig. 2).

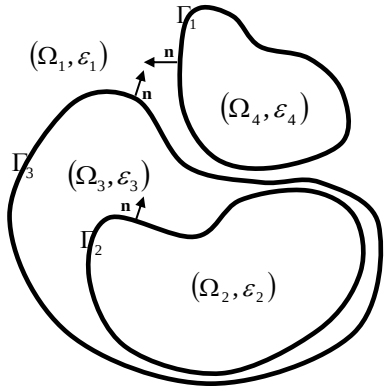

Fig. 2: Three objects and four distinct media denoted Ω_j , $j = 1-4$, with permittivity ε_j. The host medium is denoted Ω_1. Let us remark that Ω_3 is delimited by the two interfaces Γ_2 and Γ_3 . The orientation of normal vectors are defined only once regardless of the medium. The normal vectors are always directed towards the host medium.

To apply the MLFMM to each region independently, we consider that, for each material, the normal vector is always oriented towards the outside. For each triangular element of the interface discretization between two objects, one has two normal vectors $\mathbf{n}_\Gamma$ and $-\mathbf{n}_\Gamma$. One defines then the following functions,

$$j_e : \left\{ Discretiza\ tion\left(\bigcup_{a=2}^{N} \Gamma_a \right) \right\} \to \{1, \cdots, \mathrm{N}\}$$
$$T_a \mapsto j_e(T_a) = n$$

j_e is a function that is defined from the set of elementary triangles of the surface toward the environment numbers, where $e = \mathrm{int}, out$. N is the number of media. Each elementary triangle T_a of the discretization has an inside and outside number, given by functions j_{int} and j_{out} [41]. With these functions, one can write the components of matrices $[\mathbf{G}_e]$ by

$$[\mathbf{G}_e]_{a,b} = [\mathbf{G}_{j_e(T_a)}]_{a,b} \delta_{j_e(T_a) j_e(T_b)} \tag{18}$$

where δ is the Kronecker 's delta, and

$$\left[\mathbf{G}_{j_e(T_a)}\right]_{a,b} = \int_{T_b} G_{j_e(T_a)}\left(\left|\mathbf{s}_a - \mathbf{s}\right|\right) d\mathbf{s} \tag{19}$$

The matrix-vector products are given by,

$$\left[\mathbf{G}_e\right]_a \sigma_e = \sum_{b=1}^{N} \left[\mathbf{G}_{j_e(T_a)}\right]_{a,b} \sigma_{e,b} \delta_{j_e(T_a) j_e(T_b)} \tag{20a}$$

$$\left[\mathbf{H}_e\right]_a \sigma_e = \sum_{b=1}^{N} \left[\mathbf{H}_{j_e(T_a)}\right]_{a,b} \sigma_{e,b} \delta_{j_e(T_a) j_e(T_b)} \tag{20b}$$

This is however not an optimal formulation if there are objects in contact. Indeed, all contact parts will be calculated twice.

To avoid unnecessary calculations, we proceed in another way. Each elementary triangle of the discretization has only one normal vector, even for objects in contact. In the example sketched in Fig. 2, the radiated σ_{int} and $\mathbf{h}_{\text{int}}$ from the medium Ω_3 on the boundary surface Γ_2 are equal to radiated σ_{out} and $\mathbf{h}_{out}$ from the medium Ω_2. In the general case, if the triangle T_a belongs to the discretization of the common part of two objects in contact (Ω_n and Ω_m), then the equivalent surface charge and current radiated inside of Ω_n $\left(\sigma_{\text{int}}(\Omega_n, T_a)\right)$ are equal to the equivalent surface charge and current radiated outside of Ω_m $\left(\sigma_{out}(\Omega_m, T_a)\right)$, and vice versa. The matrix-vector product can thus be written:

$$\left[\mathbf{G}_e\right]_a \sigma_e = \sum_{b=1}^{N} \left[\mathbf{G}_{j_e(T_a)}\right]_{a,b} \left(\sigma_{e,b} \delta_{j_e(T_a) j_e(T_b)} + \sigma_{e',b} \delta_{j_e(T_a) j_{e'}(T_b)}\right) \tag{21}$$

Therefore, with some manipulations, one can redefine the components of the matrix $\left[\mathbf{G}_e\right]$ by

$$\left[\mathbf{G}_e\right]_{a,b} = \left[\mathbf{G}_{j_e(T_b)}\right]_{a,b} \left(\delta_{j_e(T_a) j_e(T_b)} - \delta_{j_{e'}(T_a) j_e(T_b)}\right) \tag{22a}$$

$$\left[\mathbf{H}_e\right]_{a,b} = \left[\mathbf{H}_{j_e(T_b)}\right]_{a,b} \left(\delta_{j_e(T_a) j_e(T_b)} - \delta_{j_{e'}(T_a) j_e(T_b)}\right) \tag{22b}$$

where $(e, e') = (\text{int}, out), (out, \text{int})$

The above formulations allow us to obtain an optimal MLFMM. If the objects are separated the term $\delta_{j_e(T_a) j_{e'}(T_b)}$ is zero, and one gets the expressions (18).

3. MLFMM

To implement the 3D MLFMM for multiple objects, an octree structure is introduced: the whole set of objects is introduced into a bounding cube, partitioned into eight smaller cubes of equal size. The same process is repeated recursively until a stop condition is fulfilled. The stop condition can be set, either on the edge length of the smallest subcube or on the number of triangles in the subcube, as shown in Fig. 3. Various studies have established the minimum size of leaf cells relative to wavelength [21]. In this paper, the minimum size is fixed to $d_{\min} = 0.12\,\lambda$ in order to remain valid in the high frequency domain.

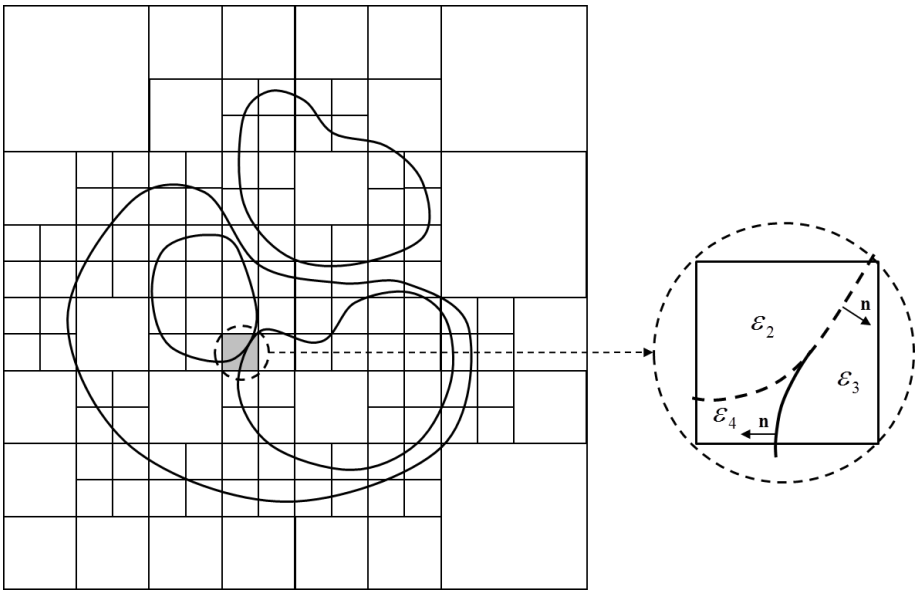

Fig. 3: Hierarchical division of all objects in an octree structure. The right figure is a zoom on the content of the grey box.

One denotes C_y^l the subcube of center y_l containing the source points and C_x^l the subcube of center x_l containing the observation points. The superscript l denotes the grouping level. A subcube can contain elementary triangles belonging to different objects and elementary triangles arising from the discretization of the contact part between two objects, as shown in the zoom of the gray box in Fig. 3. In this case, one decomposes it in several subcubes that contain triangles of the same internal or external number. This decomposition is the following

$$C_y^l(n,.)\cap\Gamma=\left\{T\in C_y^l\cap\Gamma\middle| j_{\text{int}}(T)=n\right\}$$

$$C_y^l(.,m)=\left\{T\in C_y^l\cap\Gamma\middle| j_{out}(T)=m\right\}$$

$C_y^l(n,.)$ and $C_y^l(.,m)$ respectively contain only triangles whose internal number is n and external number is m. T is the elementary triangle of the discretization.

Two subcubes are said to be near neighbors if they are at the same refinement level and share a boundary point (a subcube is a near neighbor of itself). Two subcubes are said to be far neighbors if they are at the same refinement level and are not near neighbors [11]. The matrix-vector product can be written as follows:

$$[\mathbf{G}_e]\sigma_e=[\mathbf{G}_e]_{near}\,\sigma_e+[\mathbf{G}_e]_{far}\,\sigma_e \tag{23a}$$

$$[\mathbf{H}_e]\sigma_e=[\mathbf{H}_e]_{near}\,\sigma_e+[\mathbf{H}_e]_{far}\,\sigma_e \tag{23b}$$

where $[\mathbf{G}_e]_{near}$ is the near interaction matrices, exactly calculated at all points located on the near neighborhood with the standard BEM, and $[\mathbf{G}_e]_{far}$ the far interactions matrices, approximately calculated at all points located in the far neighborhood with the MLFMM [22].

We define $suburb\left(C_x^l\right)$, the boxes of same refinement whose parent are neighbors of the parent of C_x^l. The suburbs boxes participate in the far interaction matrix-vector product, calculated by the MLFMM process, and used by the iterative solver.

One knows that

$$C_x^l\cap\Gamma=\bigcup_n C_x^l(n,.)\cap\Gamma=\bigcup_m C_x^l(.,m)\cap\Gamma$$

For all C_x^l, $\forall T_a\in C_x^l\cap\Gamma$

$$\left(\mathbf{G}_e^{far}.\sigma\right)=\sum_{C_y^l\in suburb(C_x^l)}\int_{C_y^{(l)}\cap\Gamma}G_{j_e(T_b)}\left(|x_a-y|\right)\left(\delta_{j_e(T_a)j_e(T_b)}-\delta_{j_{e'}(T_a)j_e(T_b)}\right)\sigma(y)dy \tag{24a}$$

$$\left(\mathbf{H}_e^{far}.\sigma\right)=\sum_{C_y^l\in suburb(C_x^l)}\int_{C_y^{(l)}\cap\Gamma}H_{j_e(T_b)}\left(|x_a-y|\right)\left(\delta_{j_e(T_a)j_e(T_b)}-\delta_{j_{e'}(T_a)j_e(T_b)}\right)\sigma(y)dy \tag{24b}$$

Finally, for all triangles in $C_x^l(n,.)$, the matrix-vector products are given by

$$\left(\mathbf{G}_{\text{int}}^{far}.\sigma\right)=\frac{ik_n}{16\pi^2}\int_{\mathbf{S}^2}e^{ik_n<\mathbf{s},\mathbf{x}_l\mathbf{x}>}G_{C_x^l(n,.)}(\mathbf{s})d\mathbf{s}\quad-\sum_{m\in j_{out}\{C_x^l(n,.)\}}\frac{ik_m}{16\pi^2}\int_{\mathbf{S}^2}e^{ik_m<\mathbf{s},\mathbf{x}_l\mathbf{x}>}G_{C_x^l(n,m)}(\mathbf{s})d\mathbf{s}\qquad(25a)$$

$$\left(\mathbf{H}_{\text{int}}^{far}.\sigma\right)=\frac{-k_n^2}{16\pi^2}\int_{\mathbf{S}^2}e^{ik_n<\mathbf{s},\mathbf{x}_l\mathbf{x}>}H_{C_x^l(n,.)}(\mathbf{s})d\mathbf{s}\quad+\sum_{m\in j_{out}\{C_x^l(n,.)\}}\frac{k_m^2}{16\pi^2}\int_{\mathbf{S}^2}e^{ik_m<\mathbf{s},\mathbf{x}_l\mathbf{x}>}H_{C_x^l(n,m)}(\mathbf{s})d\mathbf{s}\qquad(25b)$$

where

$$G_{C_x^{(l)}(n,.)}(\mathbf{s})=\sum_{C_y^l\in suburb\ (C_x^l)}\Pi_{j_{\text{int}}\left(C_y^{(l)}\right)}(n)T_{\mathbf{r}_l}^L(\mathbf{s})F_{C_y^{(l)}(n,.)}(\mathbf{s})\qquad(26a)$$

$$G_{C_x^{(l)}(n,m)}(\mathbf{s})=\sum_{C_y^l\in suburb\ (C_x^l)}\Pi_{j_{\text{int}}\left(C_y^{(l)}\right)}(m)T_{\mathbf{r}_l}^L(\mathbf{s})F_{C_y^{(l)}(m,.)}(\mathbf{s})\qquad(26b)$$

$$H_{C_x^{(l)}(n,.)}(\mathbf{s})=\sum_{C_y^l\in suburb\ (C_x^l)}\Pi_{j_{\text{int}}\left(C_y^{(l)}\right)}(n)T_{\mathbf{r}_l}^L(\mathbf{s})\overline{F}_{C_y^{(l)}(n,.)}(\mathbf{s})$$

(26c)

$$H_{C_x^{(l)}(n,m)}(\mathbf{s})=\sum_{C_y^l\in suburb\ (C_x^l)}\Pi_{j_{\text{int}}\left(C_y^{(l)}\right)}(m)T_{\mathbf{r}_l}^L(\mathbf{s})\overline{F}_{C_y^{(l)}(m,.)}(\mathbf{s})\qquad(26d)$$

with, for $p=n,m$

$$F_{C_y^{(l)}(p,.)}(\mathbf{s})=\int_{C_y(p,.)\cap\Gamma}e^{ik_p<\mathbf{s},\mathbf{y}\mathbf{y}_l>}\sigma(y)dy\qquad(27a)$$

$$\overline{F}_{C_y^{(l)}(p,.)}(\mathbf{s})=\int_{C_y^{(l)}(p,.)\cap\Gamma}\left(\mathbf{s}.\mathbf{n}_{C_y^{(l)}(p,.)\cap\Gamma}\right)e^{ik_p<\mathbf{s},\mathbf{y}\mathbf{y}_l>}\sigma(y)dy\qquad(27b)$$

for all $C_x^l(.,m),\ \forall T_a\in C_x^l(.,m)\cap\Gamma$

$$\left(\mathbf{G}_{ext}^{far}.\sigma\right)=\frac{ik_m}{16\pi^2}\int_{\mathbf{s}\in\mathbf{S}^2}e^{ik_m<\mathbf{s},\mathbf{x}_l\mathbf{x}>}G_{C_x^l(.,m)}(\mathbf{s})d\mathbf{s}\quad-\sum_{n\in j_{\text{int}}\{C_x^l(.,m)\}}\frac{ik_n}{16\pi^2}\int_{\mathbf{S}^2}e^{ik_n<\mathbf{s},\mathbf{x}_l\mathbf{x}>}\overline{G}_{C_x^l(n,m)}(\mathbf{s})d\mathbf{s}\qquad(28a)$$

$$\left(\mathbf{H}_{ext}^{far}.\sigma\right)=\frac{-k_m^2}{16\pi^2}\int_{\mathbf{S}^2}e^{ik_m<\mathbf{s},\mathbf{x}_l\mathbf{x}>}H_{C_x^l(.,m)}(\mathbf{s})d\mathbf{s}\quad+\sum_{m\in j_{\text{int}}\{C_x^l(.,m)\}}\frac{k_n^2}{16\pi^2}\int_{\mathbf{S}^2}e^{ik_n<\mathbf{s},\mathbf{x}_l\mathbf{x}>}\overline{H}_{C_x^l(n,m)}(\mathbf{s})d\mathbf{s}\qquad(28b)$$

where

$$G_{C_x^{(l)}(.,m)}(\mathbf{s})=\sum_{C_y^l\in suburb\ (C_x^l)}\Pi_{j_{ext}\left(C_y^{(l)}\right)}(m)T_{\mathbf{r}_l}^L(\mathbf{s})F_{C_y^{(l)}(.,m)}(\mathbf{s})\qquad(29a)$$

$$\overline{G}_{C_x^{(l)}(n,m)}(\mathbf{s}) = \sum_{C_y^l \in suburb\ (C_x^l)} \Pi_{j_{ext}(C_y^{(l)})}(n) T_{\mathbf{r}_l}^L(\mathbf{s}) F_{C_y^{(l)}(.,n)}(\mathbf{s}) \tag{29b}$$

$$H_{C_x^{(l)}(.,m)}(\mathbf{s}) = \sum_{C_y^l \in suburb\ (C_x^l)} \Pi_{j_{ext}(C_y^{(l)})}(m) T_{\mathbf{r}_l}^L(\mathbf{s}) \overline{F}_{C_y^{(l)}(.,m)}(\mathbf{s}) \tag{29c}$$

$$\overline{H}_{C_x^{(l)}(n,m)}(\mathbf{s}) = \sum_{C_y^l \in suburb\ (C_x^l)} \Pi_{j_{ext}(C_y^{(l)})}(n) T_{\mathbf{r}_l}^L(\mathbf{s}) \overline{F}_{C_y^{(l)}(.,n)}(\mathbf{s}) \tag{29d}$$

with, for $p = n, m$

$$F_{C_y^{(l)}(.,p)}(\mathbf{s}) = \int_{C_y^{(l)}(.,p)\cap\Gamma} e^{ik_p <\mathbf{s},\mathbf{y}\mathbf{y}_l>} \sigma(y) dy \tag{30a}$$

$$\overline{F}_{C_y^{(l)}(.,p)}(\mathbf{s}) = \int_{C_y^{(l)}(.,p)\cap\Gamma} \left(\mathbf{s}.\mathbf{n}_{C_y^{(l)}(.,p)\cap\Gamma}\right) e^{ik_p <\mathbf{s},\mathbf{y}\mathbf{y}_l>} \sigma(y) dy \tag{30b}$$

Integrations are performed on the unit sphere $\mathbf{S}^2$. The unit sphere discretization depends on the wave number k_p, with $p = n, m$. $\mathbf{n}_{C_x^l(p,.)\cap\Gamma}$ and $\mathbf{n}_{C_y^{(l)}(.,p)\cap\Gamma}$ are unit normal vectors of $C_x^l(p,.)\cap\Gamma$ and $C_x^l(.,p)\cap\Gamma$, respectively. $\Pi_{j_e(C_y^{(l)})}$ is the indicator function, it is defined by

$$\Pi_C(x) = \begin{cases} 1 & \text{si } x \in C \\ 0 & \text{sinon} \end{cases}$$

The translator operator is defined as

$$T_{\mathbf{r}_l}^L(\mathbf{s}, n) = \sum_{l=0}^{L} (2l+1) i^2 h_l^{(1)}(k_n \mathbf{r}_l) P_l(\cos(\mathbf{s}, \mathbf{r}_l)) \tag{31}$$

$\mathbf{r}_l = \mathbf{y}_l \mathbf{x}_l$ is the vector linking the centers of subcubes C_x^l and C_y^l. L is the number of terms for the truncation of the multipole expansion, whose choice is discussed in [21]. $h_l^{(1)}$ is the spherical Henkel function of the first kind and P_l is the Legendre polynomial of degree l.

The only problem in assembling the near matrix $[\mathbf{G}_e]_{near}$ is the singularity of Green's function for $\mathbf{x} = \mathbf{y}$. Several methods have been developed for solving this problem. Among those , one can mention the solution that consists in writing the Green's function as the sum of a regular function and a singular function [21], the solution that consists in using the

collocation points and isoparametric interpolation [46], or even the solution that consists interpolating and using the Duffy transformation [47].

Finally, the algebraic system $[\mathbf{A}]x = b$, where the matrix $[\mathbf{A}]$ is neither symmetric nor Hermitian, is obtained. The computation time necessary to solve the system, by the GMRES method, depends of the number of internal and external iterations, which in turn depends on the desired residual error. The iterative resolution of the problem needs a quite large numbers of GMRES iterations to reach a residual error of 10^{-6}. Thus, in order to accelerate the calculation, as the number of iterations is important and is a limiting factor for large size problems, a preconditioner is used.

The matrix-vector product can be written as

$$[\mathbf{A}]\mathbf{x} = \left([\mathbf{A}]_{near} + [\mathbf{A}]_{far}\right)\mathbf{x} \tag{32}$$

where $[\mathbf{A}]_{near}$ and $[\mathbf{A}]_{far}$ are the near and far interactions matrices.

The natural choice is to use the near-interaction matrix $[\mathbf{A}]_{near}$ (near-field) for preconditioning [48]. These near-interaction matrix elements are the largest in magnitude. $[\mathbf{A}]_{near}^{-1}[\mathbf{A}]$ provides a much better conditioning than $[\mathbf{A}]$, i.e. $Cond\left([\mathbf{I}] + [\mathbf{A}]_{near}^{-1}[\mathbf{A}]_{far}\right) < cond\,(\mathbf{A})$.

$$[\mathbf{A}]_{near}^{-1}[\mathbf{A}]\mathbf{x} = \left([\mathbf{I}] + [\mathbf{A}]_{near}^{-1}[\mathbf{A}]_{far}\right)\mathbf{x} \tag{33}$$

Using the incomplete factorization $ILU(\tau)$ of $[\mathbf{A}]_{near}$ drastically reduces the number of iterations [45]. The τ factor is the drop tolerance.

4. NUMERICAL RESULTS

In this section, the MLFMM is verified and its capabilities are demonstrated by considering several examples of plane waves scatted by photonic objects.

The following parameters have been used in all the computations presented hereafter.

The normalized residual error for the GMRES solver is set to 10^{-6}. The number of terms in the multipole expansion used in the MLFMM implementation is limited to $L_n = k_n D\sqrt{3} + 7.5\log(k_n D\sqrt{3} + \pi)$ [21] for dielectric objects, where D is the edge length of subcube. For low loss dielectrics, the following formula $\bar{L} = |ka\sqrt{3}| + 7.5log(|ka\sqrt{3}| + \pi)$ can be used [49]. But, for high loss dielectrics, the relative error obtained by $\bar{L}$ is greater than 10^{-4}, and L is determined adaptively. L is determined numerically at each level in the MLFMM tree so that the maximum error is below the required threshold starting, from $L = |ka\sqrt{3}|$ [49]. The matrix-vector product is approximated with a relative error of order $O(10^{-4})$. The wavelength of the plane wave is $\lambda_0 = 516.6\,nm$.

In a first step, the method is verified for a single objet. Absorption, scattering and extinction efficiencies of a gold sphere of various radii R are calculated by MLFMM (sphere of radii $R = 0.125\lambda$ to $R = 2\lambda$), and compared to Mie's theory, with good agreement (Fig. 4). Gold permittivity, is taken from Palik's handbook [50], is $\varepsilon_r = -4.125 + 2.578\,i$.

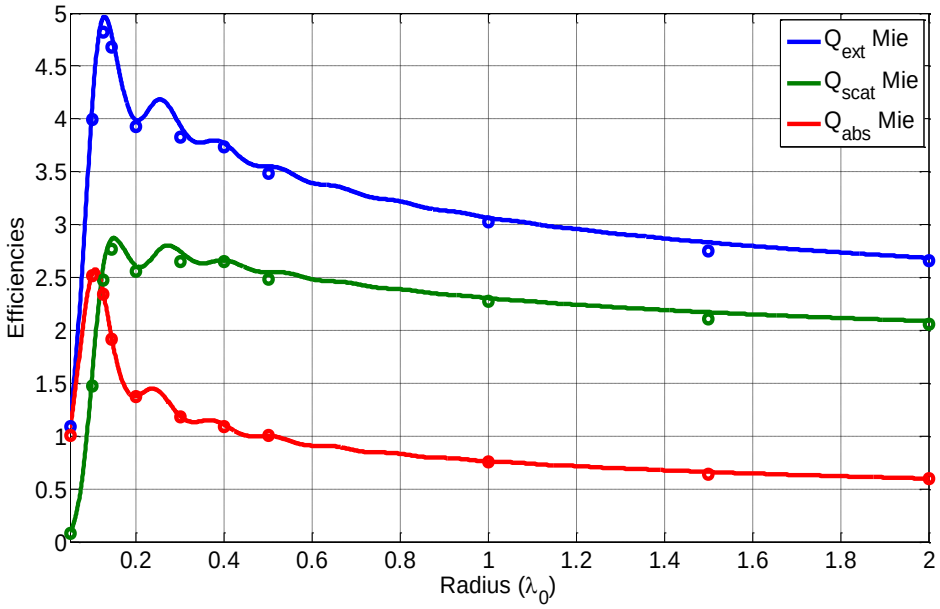

Fig. 4: (Color online) Absorption, scattering and extinction efficiencies for a gold sphere. Comparison between MLFMM and Mie's theory.

Then, the bistatic RCS of the near resonance plasmon gold sphere of radius $0.145\lambda_0$, calculated by MLFMM, is compared with Mie's theory (Fig. 5). The comparison between the BEM and MLFMM, in terms of computation time and memory, is also presented in Table 1. It clearly appears that the MLFMM is much more efficient than the BEM and can thus handle problems with larger numbers of unknowns.

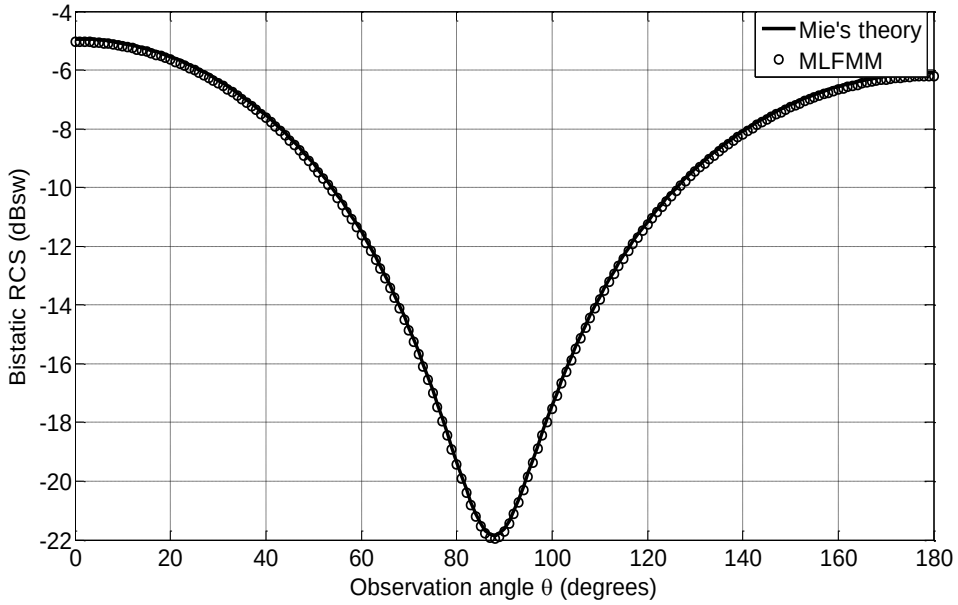

Fig. 5: Bistatic RCS for a near resonance gold sphere of radius $0.145\lambda_0$.

Rad. $(\frac{R}{\lambda_0})$	No. of unkn.	No. of Levels	No. of iter	Drop Tol (τ)	Memory (MB) BEM/MLFMM	Time (s) BEM/MLFMM	e_{ext}
0.125	13,936	2	31	10^{-2}	1,945 /152	381 /16,56	3.7 e-2
0.145	15,952	2	48	10^{-2}	2,913 /157	1,076 /23.79	4.2 e-2
0.5	37,824	2	67	10^{-2}	/1,192	/75.85	1.8 e-2
1	68,528	3	105	10^{-2}	/845	/423.8	1.02 e-2
1.5	134,608	3	151	10^{-2}	/3,399	/2,643	3.05 e-2
2	196,752	3	195	10^{-1}	/4,321	/4,801	1.07 e-2

Table 1: Number of Unknowns, Number of Levels, Drop Tolerance value, Convergence Iterations, Memory requirements and computation time for BEM and MLFMM, Relative Error of Extinction

Additional technical information on our calculations is presented in Table 1, the number of levels, the number of iterations, the drop tolerance value (τ) used for the incomplete factorization $ILU(\tau)$, the memory and time CPU calculation BEM-MLFMM and the relative error of the extinction efficiency (e_{ext}) with respect to the Mie's theory results. This relative error e_{ext} is order of $O(10^{-2})$. The average relative errors of the BEM-MLFMM solution and the matrix-vector product are respectively $O(10^{-4})$ and $O(10^{-5})$, this difference is due to the accumulation of errors (numerical integration, interpolation/anterpolation and far-zone interaction) generated in each iteration.

The convergence of the MLFMM formulation has been compared to other surface integral equation (SIE) formulations (PMCHWT, CTF, Muller, CNF and JMCFIE), for a gold nanoparticle, as studied by Araùjo et al [35]. The normalized root mean square (RMS) errors

of the extinction efficiency with respect to the Mie's theory results are shown in Fig. 6 (top) versus the number of unknowns.

It appears that, our formulation has a better convergence than the CFT formulation and a poorer convergence than the other formulations. This relatively slow convergence is not due to the MLFMM, but to the BEM formalism (Fig. 6, bottom). This could be explained by the collocation method we used, and use of basis functions could improve it.

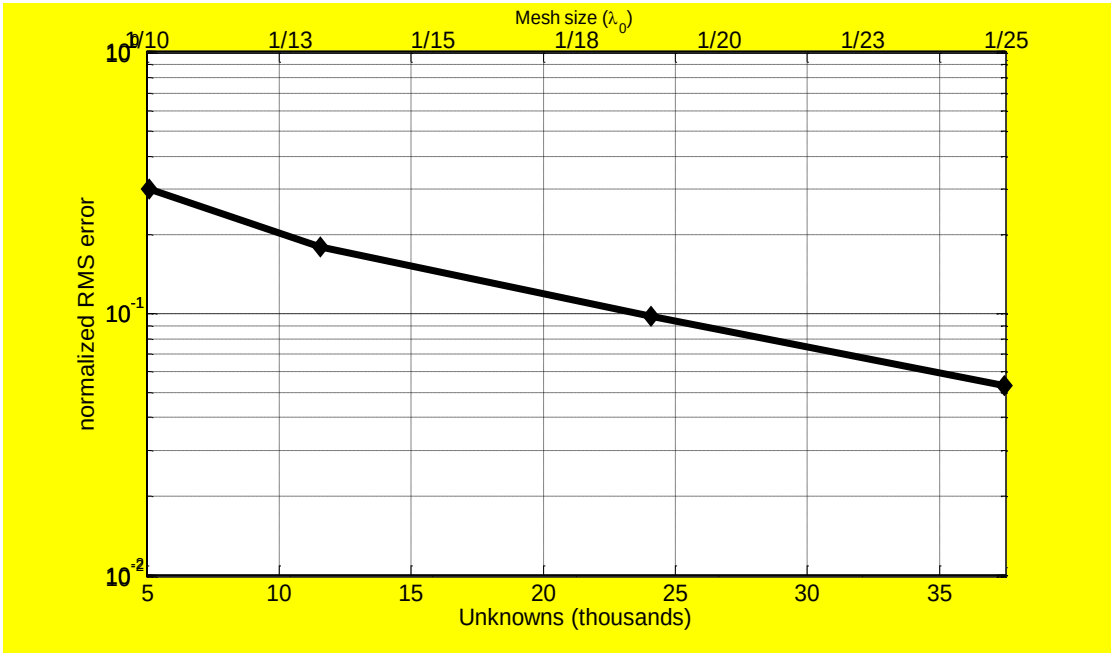

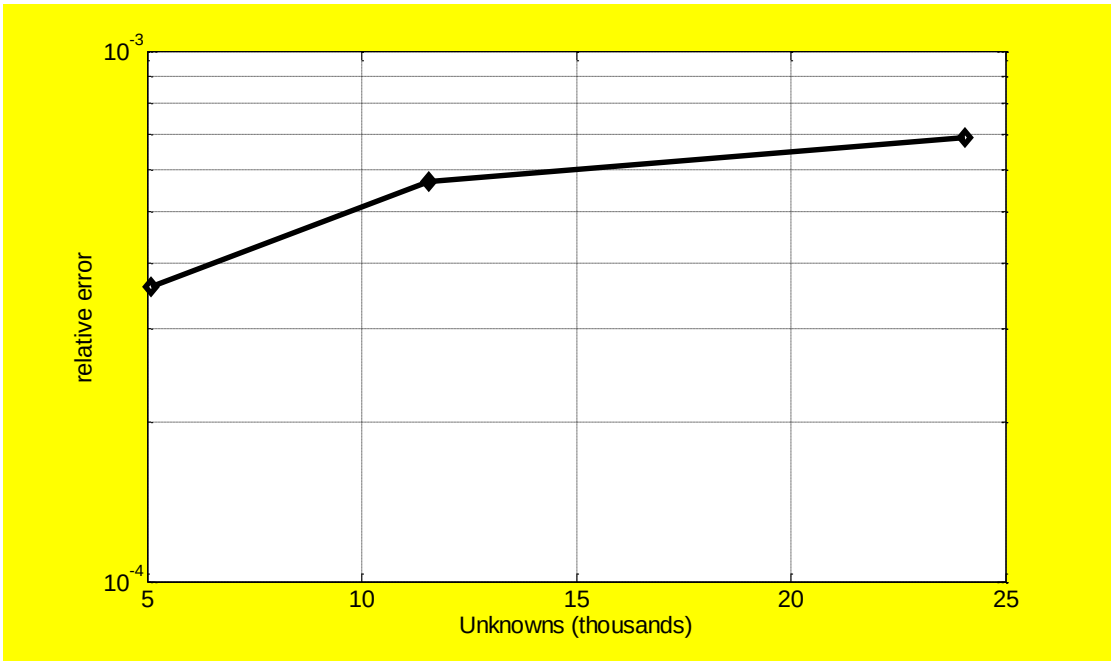

Fig. 6: (Top) Normalized RMS error (e_{rms}) of the extinction efficiency and (bottom) average relative error BEM-MLFMM of gold spheres of radius $R_1 = \lambda_0/2$ at $\lambda_0 = 548.6nm$ and $\varepsilon_r = -5.8.6 + 2.1i$.

To demonstrate the ability of our method to handle objects in contact, we consider, in the second example, the scattering of a plane wave on a gold sphere coated with a lossless dielectric shell. The radius of the gold spherical core is $R_1 = 0.145\,\lambda_0$ and the encapsulating

shell, with external radius $R_2 = 0.215\,\lambda_0$, is made of silica. As before, the dielectric constant of silica is taken from Palik handbook [50] : $\varepsilon_2 = 2.1316$. The geometry is modeled using 49,936 unknowns (6,242 triangles). We use 3 levels for the MLFMM with only 38 iterations, necessitating 1039 second of computing time and 1241 *MB* of calculation memory. The results are in good agreement with Mie's theory (Fig. 7). One remarks that modifications of plasmonic properties induced by the silica shell are well accounted for.

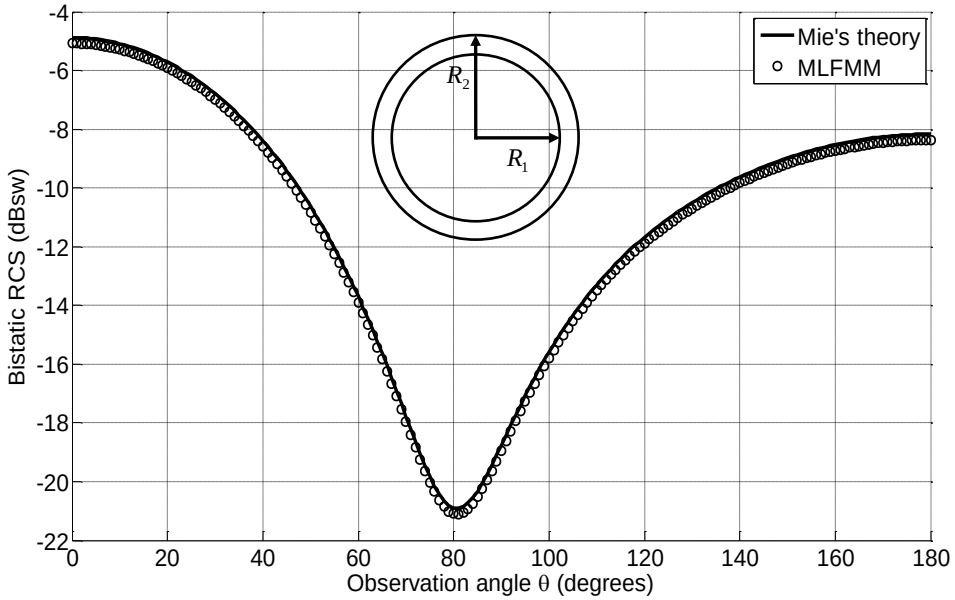

Fig. 7: Bistatic RCS of a silica coated gold sphere.

In the final numerical test, a silver-gold heterodimer is considered. The silver and gold sphere radii are respectively $R_1 = 0.183\lambda_0$ and $R_2 = 0.125\lambda_0$. The plane wave is incident along the z axis (Fig. 8 top). The bistatic RCS of the heterodimer calculated by the MLFMM is compared to BEM results (Fig. 8 bottom). The geometry is modeled using 39376 unknowns. Three levels and only 55 iterations are used for the MLFMM, necessitating 127 seconds of computing time and 1167 *MB* calculation memory.

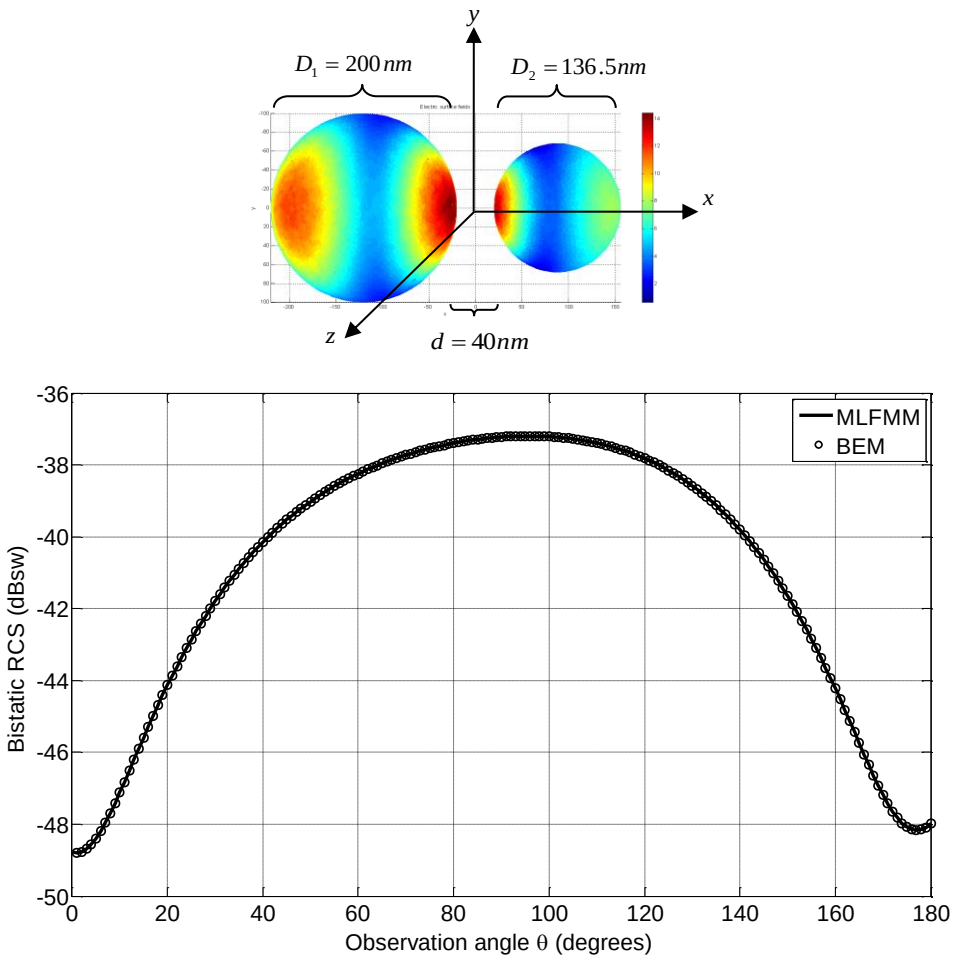

Fig. 8: (Color online) MLFMM and BEM simulation of scattering on nanoparticle Au-Ag heterodimer. (Top) Norm of the electric field represented on the surface of particles. (Bottom) Comparison of bistatic RCS MLFMM and BEM computation.

5. SUMMARY

In this paper, an original combination of the Multilevel Fast Multipole Method (MLFMM) with a potential-based Boundary Element Method (BEM) has been described. The new method is based on the scalar and vector potential BEM formulation proposed by Garcia de Abajo and Howie [41], instead of the more conventional electric and magnetic field formulations. Among other characteristics, the algorithm uses an indicator function which allows to easily take into account multiple lossy or lossless nanophotonic objects. These objects can be in contact with one another. In order to speed up the convergence, the

incomplete LU factorization of the near interaction matrix has been chosen as a preconditioner for the iterative GMRES solver.

The implementation of the formulation has been verified by comparison with prediction of Mie's theory in the case of simple spherical objects. The results obtained for absorption, scattering and extinction efficiencies of gold spherical nanoparticle, bistatic Radar Cross Section of a gold sphere near the plasmon resonance and of a silica coated gold sphere are in good agreement with the Mie's theory.

As it is fast and has low-memory requirements, the method is well suited to accurately simulate complex or large-scale optical devices, particularly plasmonic systems with large numbers of unknowns. Moreover, its convergence could be improved by using basis functions for unknown surface and charge currents within a Galerkin method, instead of the collocation method currently used.

REFERENCES

1. J.-M. Jin, *The Finite Element Method in Electromagnetics* (Wiley, 2002).
2. A. Taflove, "Review of the formulation and applications of the finite-difference time-domain method for numerical modeling of electromagnetic wave interactions with arbitrary structures," Wave Motion **10**, 547–582 (1988).
3. C. C. Cha and D. Wilkes, "Method of moments formulation for an arbitrary material configuration," in *Antennas and Propagation Society International Symposium, 1991. AP-S. Digest* (1991), pp. 1508–1511.
4. S. Rao, D. Wilton, and A. Glisson, "Electromagnetic scattering by surfaces of arbitrary shape," IEEE Transactions on Antennas and Propagation **30**, 409 – 418 (1982).
5. K. Umashankar, A. Taflove, and S. Rao, "Electromagnetic scattering by arbitrary shaped three-dimensional homogeneous lossy dielectric objects," IEEE Transactions on Antennas and Propagation **34**, 758 – 766 (1986).
6. D. Schaubert, D. Wilton, and A. Glisson, "A tetrahedral modeling method for electromagnetic scattering by arbitrarily shaped inhomogeneous dielectric bodies," Antennas and Propagation, IEEE Transactions on **32**, 77–85 (1984).

7. W.-B. Ewe, L.-W. Li, and M.-S. Leong, "SOLVING MIXED DIELECTRIC/CONDUCTING SCATTERING PROBLEM USING ADAPTIVE INTEGRAL METHOD," Progress In Electromagnetics Research **46**, 143–163 (2004).
8. Y. Shi, H. G. Wang, L. Li, and C. H. Chan, "Multilevel Green's function interpolation method for scattering from composite metallic and dielectric objects," J. Opt. Soc. Am. A **25**, 2535–2548 (2008).
9. L. Medgyesi-Mitschang, J. Putnam, and M. Gedera, "Generalized method of moments for three-dimensional penetrable scatterers," JOSA A **11**, 1383–1398 (1994).
10. V. Rokhlin, "Rapid solution of integral equations of classical potential theory," Journal of Computational Physics **60**, 187–207 (1985).
11. L. Greengard and V. Rokhlin, "A fast algorithm for particle simulations," Journal of computational physics **73**, 325–348 (1987).
12. N. Engheta, W. D. Murphy, V. Rokhlin, and M. S. Vassiliou, "The fast multipole method (FMM) for electromagnetic scattering problems," Antennas and Propagation, IEEE Transactions on **40**, 634–641 (1992).
13. R. Coifman, V. Rokhlin, and S. Wandzura, "The fast multipole method for the wave equation: A pedestrian prescription," Antennas and Propagation Magazine, IEEE **35**, 7–12 (1993).
14. C. Lu and W. Chew, "Fast algorithm for solving hybrid integral equations [EM wave scattering]," in *Microwaves, Antennas and Propagation, IEE Proceedings H* (1993), Vol. 140, pp. 455–460.
15. R. L. Wagner and W. C. Chew, "A ray-propagation fast multipole algorithm," Microwave and Optical Technology Letters **7**, 435–438 (1994).
16. J. M. Song and W. C. Chew, "Fast Multipole Method Solution Of Combined Field Integral Equation," 11TH ANNUAL REVIEW OF PROGRESS IN APPLIED COMPUTATIONAL ELECTROMAGNETICS **1**, 629–636 (1995).
17. C. C. Lu and W. C. Chew, "A multilevel algorithm for solving a boundary integral equation of wave scattering," Microwave and Optical Technology Letters **7**, 466–470 (1994).
18. L. Greengard and V. Rokhlin, "A new version of the fast multipole method for the Laplace equation in three dimensions," Acta numerica **6**, 229–269 (1997).
19. J. Song, C. C. Lu, and W. C. Chew, "Multilevel fast multipole algorithm for electromagnetic scattering by large complex objects," Antennas and Propagation, IEEE Transactions on **45**, 1488–1493 (1997).

20. H. Cheng, L. Greengard, and V. Rokhlin, "A fast adaptive multipole algorithm in three dimensions," Journal of Computational Physics **155**, 468–498 (1999).
21. E. Darve, "The fast multipole method: numerical implementation," Journal of Computational Physics **160**, 195–240 (2000).
22. N. Geng, A. Sullivan, and L. Carin, "Multilevel fast-multipole algorithm for scattering from conducting targets above or embedded in a lossy half space," Geoscience and Remote Sensing, IEEE Transactions on **38**, 1561–1573 (2000).
23. S. Velamparambil, W. C. Chew, and J. Song, "10 million unknowns: is it that big?[computational electromagnetics]," Antennas and Propagation Magazine, IEEE **45**, 43–58 (2003).
24. L. Shen and Y. Liu, "An adaptive fast multipole boundary element method for three-dimensional acoustic wave problems based on the Burton–Miller formulation," Computational Mechanics **40**, 461–472 (2007).
25. E. Darve and O. Pironneau, "Méthodes multipôles rapides: Résolution des équations de Maxwell par formulations intégrales," (1999).
26. O. Ergul and L. Gurel, "Optimal interpolation of translation operator in multilevel fast multipole algorithm," Antennas and Propagation, IEEE Transactions on **54**, 3822–3826 (2006).
27. K. C. Donepudi, J. M. Jin, and W. C. Chew, "A higher order multilevel fast multipole algorithm for scattering from mixed conducting/dielectric bodies," Antennas and Propagation, IEEE Transactions on **51**, 2814–2821 (2003).
28. J. Fostier and F. Olyslager, "An asynchronous parallel MLFMA for scattering at multiple dielectric objects," Antennas and Propagation, IEEE Transactions on **56**, 2346–2355 (2008).
29. K. Sertel and J. L. Volakis, "Multilevel fast multipole method solution of volume integral equations using parametric geometry modeling," IEEE Transactions on Antennas and Propagation **52**, 1686– 1692 (2004).
30. O. Ergul and L. Gurel, "Comparison of Integral-Equation Formulations for the Fast and Accurate Solution of Scattering Problems Involving Dielectric Objects with the Multilevel Fast Multipole Algorithm," IEEE Transactions on Antennas and Propagation **57**, 176 –187 (2009).
31. P. Yla-Oijala and M. Taskinen, "Application of combined field Integral equation for electromagnetic scattering by dielectric and composite objects," IEEE Transactions on Antennas and Propagation **53**, 1168 – 1173 (2005).

32. L. Landesa, M. G. Araújo, J. M. Taboada, L. Bote, and F. Obelleiro, "Improving condition number and convergence of the surface integral-equation method of moments for penetrable bodies," Opt. Express **20**, 17237–17249 (2012).
33. Ö. Ergül, "Fast and accurate solutions of electromagnetics problems involving lossy dielectric objects with the multilevel fast multipole algorithm," Engineering Analysis with Boundary Elements **36**, 423–432 (2012).
34. Ö. Ergül, "Analysis of composite nanoparticles with surface integral equations and the multilevel fast multipole algorithm," Journal of Optics **14**, 062701 (2012).
35. M. G. Araújo, J. M. Taboada, D. M. Solís, J. Rivero, L. Landesa, and F. Obelleiro, "Comparison of surface integral equation formulations for electromagnetic analysis of plasmonic nanoscatterers," Opt. Express **20**, 9161–9171 (2012).
36. J. M. Taboada, J. Rivero, F. Obelleiro, M. G. Araújo, and L. Landesa, "Method-of-moments formulation for the analysis of plasmonic nano-optical antennas," J. Opt. Soc. Am. A **28**, 1341–1348 (2011).
37. A. M. Kern and O. J. F. Martin, "Surface integral formulation for 3D simulations of plasmonic and high permittivity nanostructures," JOSA A **26**, 732–740 (2009).
38. M. G. Araújo, J. M. Taboada, J. Rivero, D. M. Solís, and F. Obelleiro, "Solution of large-scale plasmonic problems with the multilevel fast multipole algorithm," Optics Letters **37**, 416 (2012).
39. G. A. E. Vandenbosch, V. Volski, N. Verellen, and V. V. Moshchalkov, "On the use of the method of moments in plasmonic applications," Radio Science **46**, (2011).
40. F. Garcia de Abajo and A. Howie, "Relativistic electron energy loss and electron-induced photon emission in inhomogeneous dielectrics," Physical review letters **80**, 5180–5183 (1998).
41. F. Garcia de Abajo and A. Howie, "Retarded field calculation of electron energy loss in inhomogeneous dielectrics," Physical Review B **65**, 115418 (2002).
42. U. Hohenester and A. Trügler, "MNPBEM – A Matlab toolbox for the simulation of plasmonic nanoparticles," Computer Physics Communications **183**, 370–381 (2012).
43. U. Hohenester and J. Krenn, "Surface plasmon resonances of single and coupled metallic nanoparticles: A boundary integral method approach," Phys. Rev. B **72**, 195429 (2005).
44. U. Hohenester and A. Trugler, "Interaction of Single Molecules With Metallic Nanoparticles," IEEE Journal of Selected Topics in Quantum Electronics **14**, 1430 – 1440 (2008).

45. Y. Saad and M. H. Schultz, "GMRES: A Generalized Minimal Residual Algorithm for Solving Nonsymmetric Linear Systems," SIAM Journal on Scientific and Statistical Computing **7**, 856–869 (1986).
46. C. Pozrikidis, *A Practical Guide to Boundary Element Methods With the Software Library Bemlib*, illustrated edition (CRC Press Inc, 2002).
47. S. Mousavi and N. Sukumar, "Generalized Duffy transformation for integrating vertex singularities," Computational Mechanics **45**, 127–140 (2010).
48. K. Sertel and J. L. Volakis, "Incomplete LU preconditioner for FMM implementation," Microwave and Optical Technology Letters **26**, 265–267 (2000).
49. N. Geng, A. Sullivan, and L. Carin, "Fast multipole method for scattering from an arbitrary PEC target above or buried in a lossy half space," IEEE Transactions on Antennas and Propagation **49**, 740–748 (May).
50. E. D. Palik, *Handbook of Optical Constants of Solids* (Academic Press, 1998).